IJE TRANSACTIONS A: Basics Vol. 36 No. 07, (July 2023) 1369-1382

International Journal of Engineering

Journal Homepage: www.ije.ir

Investigation of the Damping Performance of a Shape Memory Alloy Beam

N. Danesh[a], M. J. Mahmoodabadi*[b], A. R. Fathi[c]

[a] *Department of Mechanical Engineering, University of Texas at Arlington, Arlington, TX, USA*
[b] *Department of Mechanical Engineering, Sirjan University of Technology, Sirjan, Iran*
[c] *Department of Mechanical Engineering, Babol Noushirvani University of Technology, Babol, Iran*

P A P E R I N F O

Paper history:
Received 30 December 2022
Received in revised form 09 March 2023
Accepted 10 March 2023

Keywords:
Shape Memory Alloy Beam
Energy Dissipation
Pseudo-elastic Behavior
Free Vibration
Forced Vibration

A B S T R A C T

The aim of this research is to introduce a semi-analytical approach for the analysis of the free and forced nonlinear vibrations of a bending shape memory alloy (SMA) beam; while, considering the effect of its pseudo-elastic behavior. In order to create a primary deflection, an appropriate pre-strain is applied to the SMA beam using a compression spring. A new material model was utilized to simulate the nonlinear hysteric behavior of the SMA beam, while the differential equations of motion of the beam were derived based on Euler–Bernoulli beam theory and Hamilton principle. The extracted nonlinear partial differential equations of motion are semi-analytically solved by utilizing the Galerkin method. The pseudo-elastic behavior and energy dissipation of the SMA beam were studied in the free and forced nonlinear vibration regimes. Finally, the influences of the system parameters such as the spring constant, amplitude, and frequency of the excitation force on the absorber efficiency were investigated, and its stability was studied. The numerical results depict that the SMA beam exhibits a highly nonlinear dynamical behavior, and can be used as an actuator for energy dissipation.

***doi**: 10.5829/ije.2023.36.07a.17*

NOMENCLATURE

$\boldsymbol{\varepsilon}$	Total strain	$\boldsymbol{e}$	Deviatoric strain
$\boldsymbol{\varepsilon^e}$	Thermo-elastic strain	θ	Volumetric strain
$\boldsymbol{\varepsilon^{tr}}$	Transformation strain	s	Deviatoric stress
$\boldsymbol{\varepsilon_L}$	Maximum hysteresis strain	I_i	Identify tensor
σ	Total stress	p	Volumetric stress
K	Lame constant of the material	G	Lame constant of the material
$\boldsymbol{\tau_M}$	Proper function of temperature	β	Material's parameter
$\boldsymbol{T_0}$	Initial temperature	I_{ε_L}	Indicator function of ε^{tr}
$\boldsymbol{x^{tr}}$	Transformation stress	ψ	The Helmholtz free energy
R	Radius of the elastic area in the material	u	Displacement parallel to x direction
v	Displacement parallel to y direction	w	Displacement parallel to z direction
$\boldsymbol{\pi}$	Strain energy	T	Kinetic energy
$\boldsymbol{W}$	The work is done by external force	E	Young's modulus
$\boldsymbol{I}$	Mass of inertia	η_i	The ith generalized coordinate
$\boldsymbol{\phi_i}$	The ith shape function	L	Length of the beam
$\boldsymbol{r}$	Radius of the beam	ρ	Density of the beam
$\boldsymbol{\nu}$	Material's parameter	ω	Excitation force frequency
$\boldsymbol{\varsigma}$	Loss factor	A_i	he ith vibration amplitude

1. INTRODUCTION

Special features of the smart materials that make them an appropriate choice in various fields of engineering. Among different kinds of them, Shape Memory Alloys (SMAs) have their own exclusive characteristics that make them proper alternatives to other smart substances such as piezoelectrics. Some of these features could be listed as follows:

*Corresponding Author Institutional Email
mahmoodabadi@sirjantech.ac.ir (M. J. Mahmoodabadi)

Please cite this article as: N. Danesh, M. J. Mahmoodabadi, A. R. Fathi, Investigation of the Damping Performance of a Shape Memory Alloy Beam, ***International Journal of Engineering, Transactions A: Basics***, Vol. 36, No. 07, (2023), 1369-1382

- Very effective for low frequency vibration or shape control
- Easy machinability into different shapes and sizes
- Energy dissipation more than piezoelectric materials.

These behaviors of the SMAs are related to the reversible thermo-elastic martensitic phase transformation between high symmetry, austenitic and low symmetry martensitic situations which are characterized by the superelasticity and shape memory effects. The former is the ability of a material to experience large recoverable strains without notable residual strains. The latter effect refers to the capability of restoring the original shape of materials that are plastically deformed by temperature variations. These unique characteristics provide new possibilities in use of smart materials; for example, aerospace, medical industry, vibration damping, robotics, and automotive [1-12]. Particularly, the SMA actuators can make large displacements and have a high force/weight ratio in compare with the conventional actuators. The following superiorities were also ascribed to the SMA actuators: uncomplicated design, smooth motivation, bio-adaptability, silent operation, easy actuation, and low power expenditure [13].

Extensive experimental investigations have shown that phase transformation of SMAs is a thermomechanical coupled process, with heat production due to latent heat and intrinsic dissipation [14, 15]. Based on these experimental findings, a few models that take into account thermomechanical coupling were proposed [16-19]. However, these models are either limited to small deformations [18, 19] or developed without thermal deformation gradient involved [16, 17].

In fact, at high temperature and large stress magnitude the martensite structures have a much lower Young's modulus and can be readily deformed by application of an external force or heat, indicating that thermoelastic deformations cannot be neglected [20, 21]. Due to the essential role of the beams in structural mechanics, many scientists have given particular attentions to the composition of flexible beams with SMA wires and strips. Among them, some researchers [22-31]have applied analytical solutions for studying pseudo-elastic beams, while others have used numerical approaches for them [32-34]. Razavilar et al. [35] presented a semi-analytical approach to analyze free and forced vibrations of a clamped-free SMA beam. They illustrated that the phase transformation has a significant effect on the region near the clamped end; whereas, the free end stays within the elastic domain. Hashemi and Khadem [36] analyzed dynamical behaviors of clamped-free and simply supported SMA beams. They considered the superelastic property of the SMA and introduced a mathematical model based on the Auricchio material theory. Regarding this paper, it can be concluded that there is no residual stress at the end of loading under the superelastic condition, while increasing in temperature initiates a growth in stresses at the start and end of transformation. Jose et al. [37] performed an analysis on a vibration isolator made of a SMA bar under isothermal and non-isothermal conditions. Their results exhibited that the amplitude of the response to an external excitation is limited due to the hysteretic behavior of the SMA material, while the energy of the system is well dissipated. Pan and Cho [38] proposed a shape memory alloy micro-damper to apply the pseudo-elastic behavior of NiTi wires for dissipation of the system energy. They conducted a series of tension tests to analyze the damping behavior, while the NiTi wires were subjected to different temperatures, strain rates and strain amplitudes. The experimental results displayed that the energy dissipation of the wires is practically independent of the temperature, while intensely dependent on the strain rate and amplitude. Damanpack et al. [39] investigated the vibration control ability of SMA composite beams subjected to impulsive loads by applying the 1-D model proposed by Panico and Brinson [40]. It can be seen from the results that the SMA layers with high pre-strain at low temperatures have an acceptable ability for passive vibration control. Brinson et al. [41] considered active shape control of a cantilever beam with outside-attached SMA wires. Brinston's constitutive law was used for modeling the thermo-mechanical behavior of the SMA by applying linear and nonlinear beam theories as well as temperature variations. Moallem [42] suggested a nonlinear method inspired by the sliding mode control to reduce the deflection of a flexible beam using shape memory alloy wires. On the other hand, Sohn, Han, Choi, Lee [4]] investigated vibration control and position tracking of a smart flexible system by employing SMA wire actuators and robust sliding mode control. Sayyaadi and Zakerzadeh [43] carried out a nonlinear scheme for a flexible beam with two outside-attached active SMA actuators. Andrade et al. [44] developed influences of the strain rate on stress-induced martensite, rupture strain, ultimate strength and residual strain for a CuAlMnTiB SMA. Billah et al. [45] studied the properties of the shape memory alloys suitable for the civil engineering domain and prospects of forthcoming opportunities. An integrated microstructural-mechanical model is proposed by Bellini et al. [46] for an equiatomic NiTi shape memory alloy to predict its pseudoelastic cyclic behaviour.

The aim of the current study is to investigate the dynamical behavior of a simply supported SMA beam with a compression spring to make a pre-strain on it. The three-dimensional constitutive material model presented by Souza et al. [47] is utilized to simulate the hysterical behavior of the SMA, and a semi-analytical method is introduced to analyze the dynamical behavior of the system. It should be noted that most of the previous researches have been focused on the composite beams embedded with the SMA wires, and in other few cases, finite element methods have been implemented for

analyzing. Unlike these works, the current contribution proposes a novel scheme to acquire the state-space equations of the regarded SMA structure for modeling and design of a control system. The advantages of this strategy are reducing the number of required equations and decreasing the computational time.

The organization of this article is as follows. In section 2, the structure of the considered SMA beam as well as the Souza model [47] and its mathematical equations are reviewed. Moreover, the nonlinear formulation of the SMA beam under a compression force is derived in this section. The simulation and results are presented in section 3. Finally, section 4 concludes the paper.

2. SMA DAMPER AND ITS STRUCTURE

Most of the shape memory alloy actuators have been made of shape memory alloy wires or rods [47, 48]. In this research, an SMA actuator is proposed that works based on the bending of a shape memory alloy beam. The suggested system has a higher force/weight ratio and can undergo more amounts of the force in comparison with the wire or rod types. It contains a shape memory alloy beam under an excitation force (Figure 1) as well as a compression spring attached to it. The spring produces a pre-strain to create a reversible plastic deformation in the beam and to associate with a phase transformation between the twinned and detwinned martensite phases. By passing the electrical current through the SMA beam, its temperature would increase (because of the beam's electrical resistance). Increasing the temperature causes the transformation from the detwinned martensite phase to the austenite phase, which returns the beam to its original shape. By switching off the electrical current and decreasing the beam temperature, the spring changes the beam shape back again, and its phase would change to twinned martensite.

2. 1. Material Model As it was mentioned before, the most important and complicated phenomenon of SMA materials is the metallurgical phase transformation which has a significant effect on its performance. The prediction of the phenomenological hysteretic behavior of the SMAs can be understood from their governing mathematical models [49-51]. Based on the experimental observations, there are two points of view about phenomenological constitutive models, i.e., microscopic and macroscopic [52-58]. The microscopic models are applied to realize fundamental principles in the molecular scale, but those are not good choices for the structural scale. On the other hand, the macroscopic models, related to the phenomenological features of the SMA, are able to represent phase transformation kinetics using simple mathematical functions [59-64]. To name but a few, Simo and Taylor [65] developed a stable algorithm based on a return mapping approach for plane stress elastoplasticity in large time steps. Bertram [66] suggested a three-dimensional thermomechanical model based on an expanded classical theory of plasticity to describe shape memory effects as an explanation of incremental iterations. Leclercq [67] extended a phase transition model to simulate the behavior of the SMA with isothermal or non-isothermal loadings. Further, Souza, Mamiya and Zouain [47] proposed a three-dimensional model having superelasticity behaviors and shape memory effects by means of plasticity concepts.

In this study, Souza's material model [47] is used to identify the hysteric behavior of the SMA based on the theory of irreversible thermodynamics under small deformations. According to this model, a series of external and internal variables illustrate the thermo-dynamical state of a homogenized volume element at each moment. In this way, the total strain is divided into elastic and inelastic parts as follows:

$$\varepsilon = \varepsilon^{te} + \varepsilon^{tr} \quad (1)$$

where, ε, ε^{te} and ε^{tr} are the total, thermo-elastic and transformation strains, respectively. Moreover, strain ε and stress σ are decomposed as follows:

$$\varepsilon = e + \frac{\theta}{3} I_i \quad (2)$$

$$\sigma = s + pI_i \quad (3)$$

where, e is the deviatoric strain, θ = tr(ε) denotes the volumetric strain, s represents the deviatoric stress, $p = tr(\sigma)/3$ signifies the volumetric stress, and I_i indicates the identity tensor.

In this model, volumetric θ and deviatoric e strains, as well as temperature T are determined as the control variables, while transformation strain ε^{tr} is regarded as an internal variable. The transformation strain is with the phase transformation from the twinned martensite to the detwinned martensite. Due to the phase transformation, the norm of ε^{tr} is zero when the material is without oriented martensite and has maximum value ε_L when the material is completely transformed into the martensite as follows:

$$\|\varepsilon^{tr}\| \leq \varepsilon_L \quad (4)$$

where, $\|\varepsilon^{tr}\|$ shows the Euclidean norm of the transformation strain.

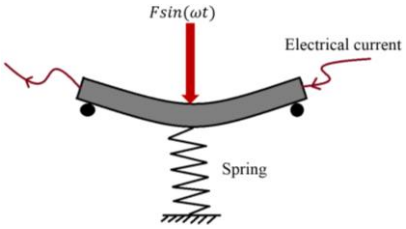

Figure 1. Schematic of the considered shape memory alloy beam

In this model, the Helmholtz free energy, suggested by Souza [47], could be represented as follows:

$$\psi(\theta,\varepsilon,\varepsilon^{tr},T)=\frac{1}{2}K\theta^2+G\|\varepsilon-\varepsilon^{tr}\|^2+\tau_M(T)\|\varepsilon^{tr}\|+\frac{1}{2}h\|\varepsilon^{tr}\|^2+I_{\varepsilon_L}(\|\varepsilon^{tr}\|) \quad (5)$$

In Equation (5), K and G signify the Lame constants of the material, $\tau_M(T)$ denotes a function of temperature, and h represents a material parameter related to its hardening. $\tau_M(T)$ is considered as $\tau_M(T)=\beta\langle T-T_0\rangle$, where β is a constant parameter, T_0 shows an initial temperature, and operator '$\langle.\ \rangle$' illustrates the positive part of a function.

In addition, function I_{ε_L} is defined as follows:

$$I_{\varepsilon_L}(\|\varepsilon^{tr}\|)=\begin{cases}0 & if\ \ \|\varepsilon^{tr}\|\le\varepsilon_L\\ +\infty & otherwise\end{cases} \quad (6)$$

From Equation (5), the following constitutive relations could be written.

$$p=\frac{\partial\psi}{\partial\theta}=K\theta \quad (7)$$

$$s=\frac{\partial\psi}{\partial\varepsilon}=2G(\varepsilon-\varepsilon^{tr}) \quad (8)$$

$$x^{tr}=-\frac{\partial\psi}{\partial\varepsilon^{tr}}=s-x \quad (9)$$

where, x^{tr} indicates the transformation stress having the following relation.

$$x=[\tau_M(T)+h\|\varepsilon^{tr}\|+\gamma]\frac{\varepsilon^{tr}}{\|\varepsilon^{tr}\|} \quad (10)$$

where,

$$\begin{cases}\gamma=0 & if\ \|\varepsilon^{tr}\|<\varepsilon_L\\ \gamma\ge 0 & if\ \|\varepsilon^{tr}\|=\varepsilon_L\end{cases} \quad (11)$$

The following equation is regarded for satisfying the second law of thermodynamics:

$$\dot{\varepsilon}^{tr}=\dot{\zeta}\frac{\varepsilon^{tr}}{\|\varepsilon^{tr}\|} \quad (12)$$

Based on the evolution of the phase transformation, f is determined as follows:

$$f=\|x^{tr}\|-R \quad (13)$$

where, R is the radius of the elastic area in material.
Finally, Souza's model [47] would be accomplished if the stability and Kuhn-Tucker conditions are satisfied, therefore.

$$\dot{\zeta}\ge 0,\quad f\le 0,\quad \dot{\zeta}f=0 \quad (14)$$

2. 1. 1. Return Mapping In this sub-section, a return mapping algorithm is presented to merge Equations (7) through (13) within the imperceptible plasticity situation. Generally, the solving procedure includes three steps as follows:

(i) A trial state and an elastic behavior are assumed for the material.
(ii) Comparing whether the calculated trial state is actually elastic.
(iii) If the trial state does not have any elastic behavior, then the state variables are designed to validate all the constraints enforced by the problem.

In this algorithm, prescribed strain ε_{n+1} is determined as a mechanical loading for the SMA material. At first, the algorithm calculates the trial state $(s_{n+1}^{trial}, x_{n+1}^{trial})$ and then the elastic condition is assumed by making $\varepsilon_{n+1}^{tr^{trial}}=\varepsilon_n^{tr}$. Therefore, by employing Equation (4), the following relations are found.

$$s_{n+1}^{trial}=2G\left(\varepsilon_{n+1}-\varepsilon_{n+1}^{tr^{trial}}\right) \quad (15)$$

$$x_{n+1}^{trial}=s_{n+1}^{trial}-\left(\tau_M(T)+h\left\|\varepsilon_{n+1}^{tr^{trial}}\right\|\right)\frac{\varepsilon_{n+1}^{tr^{trial}}}{\left\|\varepsilon_{n+1}^{tr^{trial}}\right\|} \quad (16)$$

The material has an elastic behavior if the following conditions are satisfied.

$$\begin{cases}0<\|\varepsilon_n^{tr}\|<\varepsilon_L\\ \left\|x_{n+1}^{trial}\right\|\le R\end{cases} \quad (17)$$

If $\varepsilon_n^{tr}=0$, trial force x_{n+1}^{trial} cannot be calculated by Equation (16), whereas s_{n+1}^{trial} could be computed by Equation (15). The elastic behavior would occur in the parent phase, if:

$$\begin{cases}\varepsilon_n^{tr}=0\\ s_{n+1}^{trial}\le\tau_M(T)+R\end{cases} \quad (18)$$

Finally, the case for which $\|\varepsilon_n^{tr}\|=\varepsilon_L$ has to be considered. Here, the step is elastic whenever there exists $\gamma\ge 0$ such that:

$$\begin{cases}\|\varepsilon_n^{tr}\|=\varepsilon_L\\ \|\hat{s}+\hat{\gamma}n\|\le R\quad n=-\frac{\varepsilon_{n+1}^{tr^{trial}}}{\left\|\varepsilon_{n+1}^{tr^{trial}}\right\|},\\ \hat{s}=\left\|s_{n+1}^{trial}+(\tau_M(T)+h\varepsilon_L)n\right\|,\ \hat{\gamma}=<-\hat{s}.n>\end{cases} \quad (19)$$

The step would be elastic, if one of the three conditions mentioned in Equations (17), (18) or (19) holds. At time $n+1$, the actual state is a trial state; therefore, the following relations could be mentioned.

$$\begin{aligned}\varepsilon_{n+1}^{tr}&=\varepsilon_{n+1}^{tr^{trial}}\\ s_{n+1}&=s_{n+1}^{trial}\end{aligned} \quad (20)$$

Finally, if none of conditions stated in Equations (17), (18) or (19) are approved, a phase transformation would occur, and ε_{n+1}^{tr} could be calculated by the following equation.

$$R\frac{\varepsilon_{n+1}^{tr}-\varepsilon_n^{tr}}{\|\varepsilon_{n+1}^{tr}-\varepsilon_n^{tr}\|}-2G(\varepsilon_{n+1}-\varepsilon_{n+1}^{tr})+(\tau_M(T)+h\|\varepsilon_{n+1}^{tr}\|)\frac{\varepsilon_{n+1}^{tr}}{\|\varepsilon_{n+1}^{tr}\|}=0 \quad (21)$$

If $\|\varepsilon_{n+1}^{tr}\| > \varepsilon_L$, then the solution for ε_{n+1}^{tr} and γ_{n+1} can be achieved via the following set of nonlinear equations:

$$\begin{Bmatrix} R\frac{\varepsilon_{n+1}^{tr}-\varepsilon_n^{tr}}{\|\varepsilon_{n+1}^{tr}-\varepsilon_n^{tr}\|} - 2G(\varepsilon_{n+1}-\varepsilon_{n+1}^{tr}) + \\ (\tau_M(T)+h\varepsilon_L+\gamma_{n+1})\frac{\varepsilon_{n+1}^{tr}}{\|\varepsilon_{n+1}^{tr}\|} \\ \|\varepsilon_{n+1}^{tr}\|-\varepsilon_L \end{Bmatrix} = 0 \quad (22)$$

$$s_{n+1} = 2G(\varepsilon_{n+1}-\varepsilon_{n+1}^{tr}) \quad (23)$$

2. 2. Constitutive Equation of the Shape Memory Alloy Beam In this study, the Euler-Bernoulli beam with the circular cross-section is considered to derive the set of the governing equations for simulation of the SMA system behavior using a semi-analytical solution method. While the transverse displacement of the centerline of the beam is *w*, the displacement of any points in the cross-section is *w* too. As shown in Figure 2, the plane sections stay normal to the centerline.

$$u = -z\frac{\partial w(x,t)}{\partial x} \quad v = 0 \quad w = w(x,t) \quad (24)$$

where, u, v and w designate the components of displacement in *x*, *y* and z directions, respectively. The components of the strain and stress corresponding to this displacement field are given by the following equations:

$$\begin{gathered} \varepsilon_{xx} = \frac{\partial u}{\partial x} = -z\frac{\partial^2 w(x,t)}{\partial x^2},\ \varepsilon_{yy}=0\ ,\ \varepsilon_{zz}=0\ ,\ \varepsilon_{xy}=0\ ,\ \varepsilon_{xz}=0\ ,\ \varepsilon_{yz}=0 \\ \sigma_{xx} = -Ez\frac{\partial^2 w(x,t)}{\partial x^2},\quad \sigma_{yy}=0\ ,\ \sigma_{zz}=0\ ,\ \sigma_{xy}=0\ ,\ \sigma_{xz}=0\ ,\ \sigma_{yz}=0 \end{gathered} \quad (25)$$

The strain energy of the system (π) as well as its kinetic energy (T) can be expressed as:

$$\pi = \frac{1}{2}\iiint \sigma_{xx}\varepsilon_{xx}dV = \frac{1}{2}\iiint E(\varepsilon-\varepsilon^{tr})^2 dV \quad (26)$$

$$T = \frac{1}{2}\int_0^L \rho A\left(\frac{\partial w(x,t)}{\partial t}\right)^2 dx \quad (27)$$

The work done by the mechanical load (F_0), excitation force ($Fsin(\omega t)$) and simple spring (F_k) is given by:

$$W = \int_0^L \left(F_0\left(\frac{L}{2},t\right) + F\left(\frac{L}{2},t\right)sin(\omega t) - F_k\left(\frac{L}{2},t\right)\right) w(x,t)dx \quad (28)$$

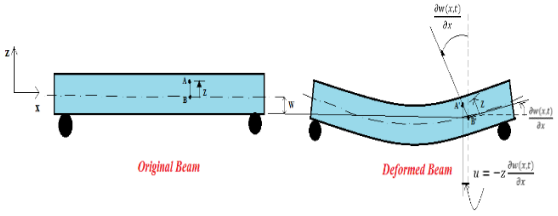

Figure 2. Bending of an Euler–Bernoulli beam

where, ω is the frequency of the excitation force. The dirac delta function could be employed to enter these forces into the equation as follows:

$$\begin{gathered} F_0\left(\frac{L}{2},t\right) = f_0\,\delta\left(x-\frac{L}{2}\right), \\ F\left(\frac{L}{2},t\right)sin(\omega t) = fsin(\omega t)\,\delta(x-\frac{L}{2}), \\ F_k\left(\frac{L}{2},t\right) = f_k\left(\frac{L}{2},t\right)\delta\left(x-\frac{L}{2}\right) \end{gathered} \quad (29)$$

In order to extract the governing equations of the motion and boundary conditions for the SMA beam, the Hamilton's principle is utilized as follows:

$$\delta\int_{t_1}^{t_2}(\pi - T - W)\,dt = 0 \quad (30)$$

where, δ denotes the variation operator, and $[t_1,\ t_2]$ describes an arbitrary time interval. By substituting Equations (26), (27), (28) and (29) into Equation (30), the following equation is obtained.

$$\begin{gathered} \int_{t_1}^{t_2}\int_0^L EI\frac{\partial^4 w(x,t)}{\partial x^4}\delta w(x,t)dx\,dt + \\ \int_{t_1}^{t_2}\left[EI\frac{\partial^2 w(x,t)}{\partial x^2}\delta\left(\frac{\partial w(x,t)}{\partial x}\right)\Big|_0^L\right]dt + \\ \int_{t_1}^{t_2}\int_0^L\frac{\partial^2 Q}{\partial x^2}dx\,dt + \int_{t_1}^{t_2} EQ\,\delta\left(\frac{\partial w(x,t)}{\partial x}\right)\Big|_0^L dt + \\ \int_{t_1}^{t_2}\int_0^L \rho A\frac{\partial^2 w(x,t)}{\partial t^2}\delta w(x,t)\,dx\,dt - \\ \int_{t_1}^{t_2}\int_0^L\left(F_k\left(\frac{L}{2},t\right) - F_0\left(\frac{L}{2},t\right) - \right. \\ \left. F\left(\frac{L}{2},t\right)sin(\omega t)\right)\delta w(x,t)\,dx\,dt = 0 \end{gathered} \quad (31)$$

where, $Q = \int \varepsilon^{tr} z\,dA$. Therefore, the differential equation of motion for the SMA beam would be presented as follows:

$$EI\frac{\partial^4 w(x,t)}{\partial x^4} + E\frac{\partial^2 Q}{\partial x^2} + \rho A\frac{\partial^2 w(x,t)}{\partial t^2} - F_0\left(\frac{L}{2},t\right) - F\left(\frac{L}{2},t\right)sin(\omega t) + F_k\left(\frac{L}{2},t\right) = 0 \quad (32)$$

While the boundary conditions are:

$$\begin{gathered} w(x,t)_{x=0} = 0 \\ w(x,t)_{x=L} = 0 \\ \left[EI\frac{\partial^2 w(x,t)}{\partial x^2} + EQ\right]_{x=0} = 0 \\ \left[EI\frac{\partial^2 w(x,t)}{\partial x^2} + EQ\right]_{x=L} = 0 \end{gathered} \quad (33)$$

The solution for Equation (32) can be regarded as:

$$w(x,t) = \sum_{i=1}^{n}\eta_i(t)\,\phi_i(x) \quad (34)$$

where, $\eta_i(t)$ and $\phi_i(x)$ denote the ith generalized coordinate and shape function, respectively. For this problem, the following form for the shape function is introduced that satisfies the boundary conditions.

$$\phi_i(x) = \sin\left(\frac{i\pi x}{L}\right) \quad (35)$$

Therefore, the following equation would be achieved.

$$W(X,\tau) = \sum_{i=1}^{n} \eta_i(\tau)\ sin(i\pi X) \quad (36)$$

Besides, the following non-dimensional parameters are selected.

$$X = \frac{x}{L},\ W(X,\tau) = \frac{w(x,t)}{L}, Z = \frac{z}{r},\quad \tau = \omega_0 t,\quad \omega = \left(\frac{\pi}{L}\right)^2 \sqrt{\frac{EI}{\rho A}} \quad (37)$$

In this study, the Galerkin method is used to change the partial differential equation to an ordinary differential equation [60]. In this way, if Equation (36) is substituted into Equation (32), and by applying Equation (37), the following nonlinear differential equation is achieved.

$$\frac{1}{2}\eta_i(\tau)(i\pi)^4 - \frac{4L\pi i^2}{R}\int_0^1 \sin(i\pi X)\,(\int \varepsilon^{tr} Z dA)dX + \frac{1}{2}\ddot{\eta}_i(\tau)(\pi)^4 - \frac{f_0 L^3}{EI} sin\left(\frac{i\pi}{2}\right) - \frac{fL^3}{EI} sin(\tau)\sin\left(\frac{i\pi}{2}\right) + \frac{KL^3}{EI}\sum_{j=1}^{n}\eta_j(\tau)\, sin\left(\frac{j\pi}{2}\right) sin\left(\frac{i\pi}{2}\right) = 0 \quad (38)$$

where, ε^{tr} could be computed by using Equation (22). Therefore,

$$\ddot{\eta}_i(\tau) = -\eta_i(\tau) i^4 + \frac{8Li^2}{R\pi^3}\int_0^1 sin(i\pi X)(\int \varepsilon^{tr} Z dA)dX + \frac{2f_0 L^3}{EI\pi^4} sin\left(\frac{i\pi}{2}\right) + \frac{2fL^3}{EI\pi^4} sin(\tau)\, sin\left(\frac{i\pi}{2}\right) - \frac{2KL^3}{EI\pi^4}\sum_{j=1}^{n}\eta_j(\tau)\, sin\left(\frac{j\pi}{2}\right) sin\left(\frac{i\pi}{2}\right) \quad (39)$$

3. SIMULATION RESULTS AND DISCUSSIONS

In this section, the fourth-order Runge–Kutta method is implemented to solve the semi-analytical equation found by the Galerkin approach in section 2 for computing the strain, transformation strain, and stress quantities. Furthermore, the considered SMA beam has length $15\ mm$ and diameter $1.5\ mm$. The spring constant is $100\ [^{N}/_{mm}]$, and results are presented for Nitinol alloy having the mechanical properties mentioned in Table 1 [47].

TABLE 1. Mechanical properties of Nitinol alloy implemented for simulations [44]

Value	Parameter
6450	$\rho\ (^{Kg}/_{m^3})$
0.33	ν
70000	$E\ (MPa)$
0.03	ε_L
253.15	$T_0\ (°K)$
323.15	$T\ (°K)$
45	$R\ (MPa)$
7.5	$\beta\ (^{MPa}/_{°K})$
500	$h\ (MPa)$

In the following, at first, the static behavior of the SMA beam is studied. Then, the dynamical behaviors of both ordinary and SMA beams are presented to investigate the effects of the SMA on the beam performance.

3. 1. Analysis of the Static Behavior In order to analyze the static behavior of the beam, it is meshed in two dimensionless directions X and Z (51×15). According to the mesh convergence study performed by the authors, the appropriate meshing steps in both directions were obtained as $\Delta X = 0.02\ and\ \Delta Z = 0.07$. Figure 3 shows the static behavior of the SMA beam with distribution load $f_0 = -35\ [N]$ and spring constant $K =$

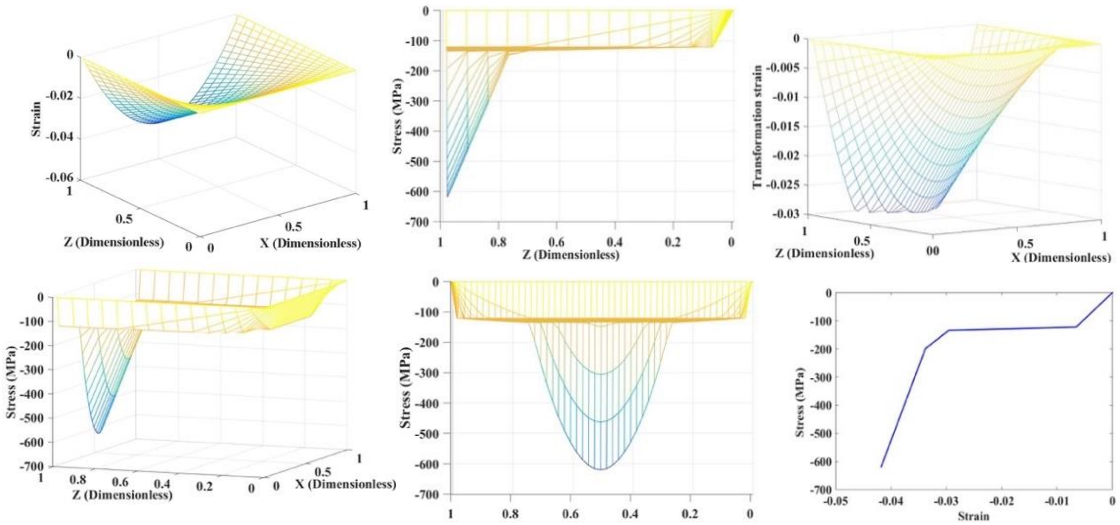

Figure 3. Static behavior of the introduced SMA beam with distribution load $f_0 = -35\ [N]$ and spring constant $K = 0$.

0. In this figure, contour map of strain, stress, and transformation strain which show all aspects of the beam behavior are being taken into consideration. As it is demonstrated, the stress distribution along direction X is symmetric. Furthermore, in order to valid the found results, Figure 4 illustrates a hysteresis loop appeared in the SMA stress-strain static response by applying variable distribution load $f_0 = -35\sin(i\pi)\,[N],\ i \in [0,2]$ and spring constant $K = 0$. As it is represented in this figure, the hysteresis loop has the same behavior as Souza's model [47].

3. 2. Analysis of the Dynamic Behavior

3. 2. 1. Free Vibration The damping property of the regarded structure is analyzed by comparing the vibration response of the SMA beam with an elastic one. Furthermore, this comparison helps to illustrate the effect of energy dissipation mechanism of SMA materials due to their hysteresis property. To this end, the SMA beam is subjected to an initial deflection which undergoes phase transformation within the SMA beam. The amount of this initial deflection is set so that the beam deflection remains on the validity domain of the Euler-Bernoulli beam theory. Figure 5 depicts the free vibration response of an elastic (non-SMA) beam for $f_0 = -15[N]$ and $K = 0$. It can be seen from this figure that there is no decreasing in the vibration amplitude (undamped harmonic response). The steady state response of the results illustrates that the SMA beam vibrates as an elastic member and its frequency is the same as its equivalent elastic beam. This behavior can be explained by the stress/strain variations as shown in Figure 6. Whereas Figure 6 exhibits the free vibration [67, 68] of the SMA beam when the temperature of the beam is $323.15°K$ and the spring has an initial compression force $f_0 = -15[N]$. At this temperature, the austenite phase is active, and the initial compression is so high. Therefore, the phase transformation from austenite to martensite would be initially induced within the beam. Hence, the hysteresis loop, depicted in Figure 6(a), makes an intense decreasing for the vibration amplitude. This process continues until the vibration amplitude cannot make any other phase transformation; therefore, the elastic response is activated only for the SMA beam. In this way, the whole beam vibrates elastically with a constant amplitude around steady state deflection $Z = -0.045$. As it is illustrated in Figure 6, the nonlinear behavior of the SMA does not affect the natural frequency of the system, and it remains constant. Indeed, there is only one damping term which is effective and practical for vibration control. In this study, contour map of strain, stress, and transformation strain which show all aspects of the beam behavior are being taken into consideration. In the free vibration study, as shown in Figure 6, an adequate initial condition was imposed onto the system to make it undergo phase transformation over the beam. The strain contour map and longitudinal distribution of strain in each layer of the cross section are depicted in Figure 6 for early oscillations when SMA beam is fully deflected.

The corresponding loss factor could be calculated by employing the following logarithmic relation.

$$\varsigma = \frac{1}{2\pi r}\ln\left(\frac{A_i}{A_{i+r}}\right) \tag{40}$$

where, A_i and A_{i+r} are vibration amplitudes ith and $(i+r)$th, respectively. In order to investigate the effect of the shape memory alloy on the vibrating behavior of the beam, the time responses of the dissipated energy for the SMA beam are generated in Figure 7. It can be seen from this figure that the total dissipated energy reduces over time until the zero value is attained.

These observations could be verified through the results presented in Figure 6. Indeed, the diagrams in Figure 6 clearly depict that the oscillation amplitude and the total energy of the system decrease via the generated hysteresis loops. The vibration amplitude of the beam becomes constant in the steady state condition, as shown in Figure 6. Figure 7 depicts the dissipated energy of the SMA beam with respect to time for the free vibrations.

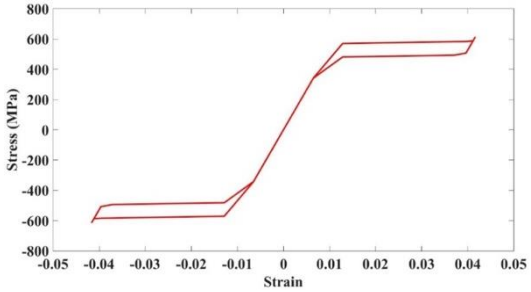

Figure 4. Stress-strain diagram to study the static behavior of the SMA beam with variable distribution load $f_0 = -35\sin(i\pi)\,[N]$, $i \in [0,2]$ and spring constant $K = 0$

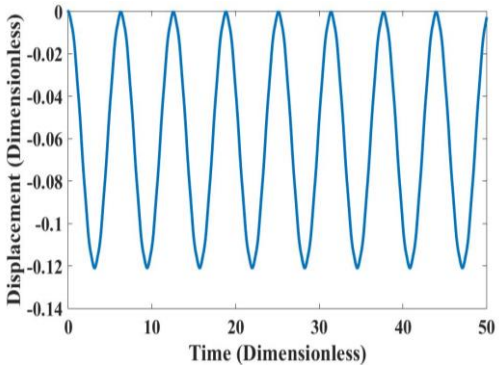

Figure 5. Free vibration of the midpoint of an ordinary beam with initial compression force $f_0 = -15[N]$ and spring constant $K = 0$

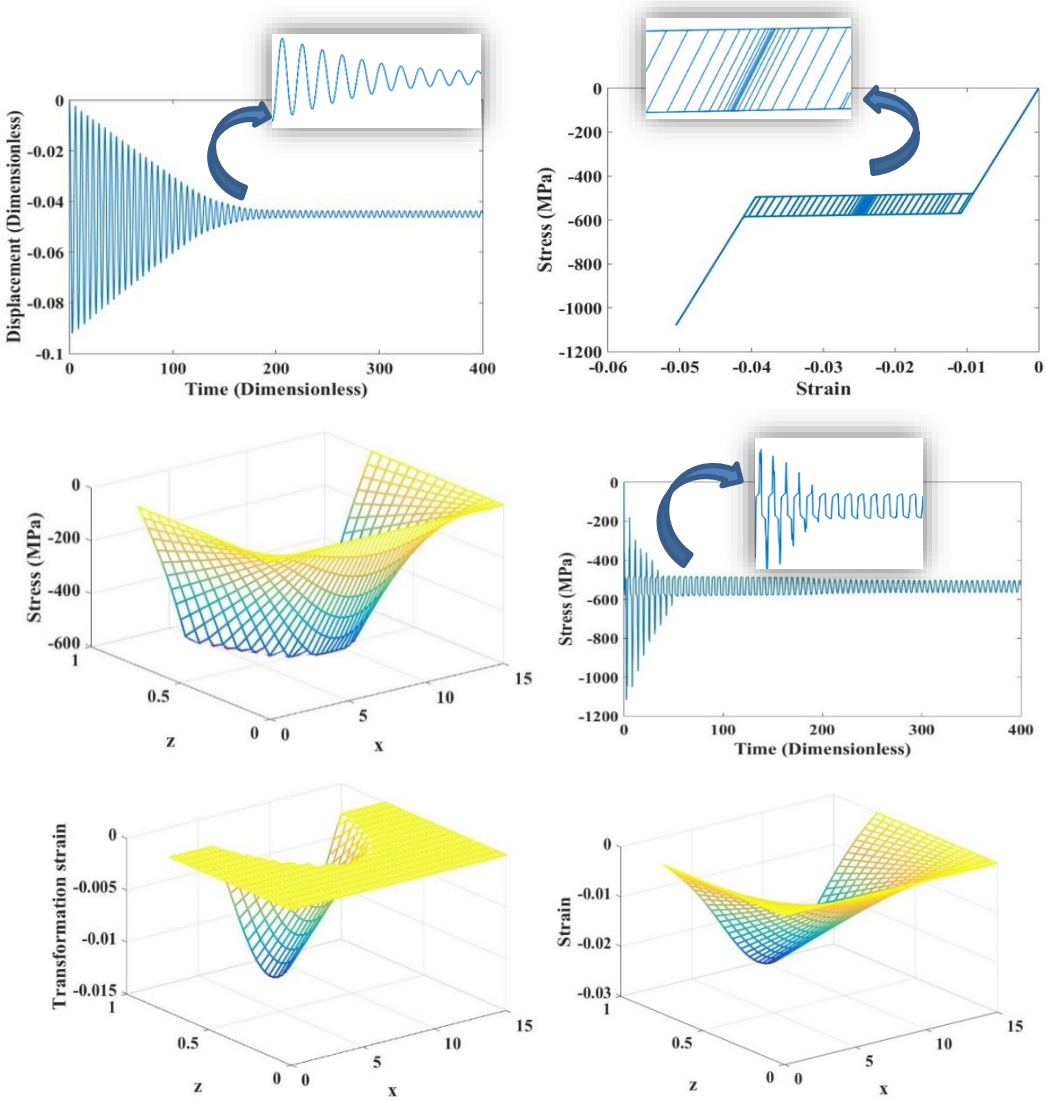

Figure 6. Dynamical behavior of the proposed SMA beam for free vibration with compression force $f_0 = -15\ [N]$ spring constant and $K = [100\ ^{N}/_{mm}]$

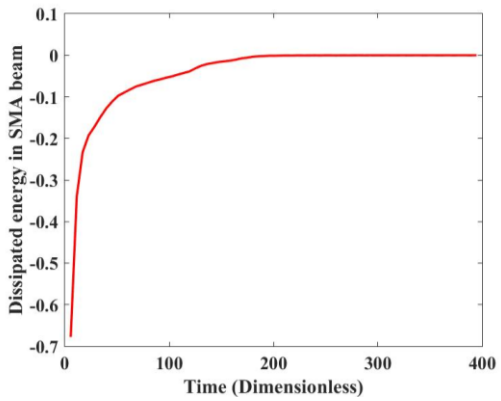

Figure 7. Dissipated energy related to the SMA beam versus time for free vibration.

Moreover, the phase plane diagram for the free vibration of the midpoint is plotted in Figure 8. This figure displays the pseudo elastic behavior of the SMA beam at the beginning of the vibration, whereas the elastic behavior can be seen at the end of the vibration.

3. 2. 2. Forced Vibration In this sub-section, the forced vibration behavior of the proposed SMA beam with excitation force $F = -15 \sin\left(\frac{3\omega_0}{4} t\right)[N]$ and spring constant $K = 100[^{N}/_{mm}]$ is investigated. The stress-strain diagram demonstrated in Figure 9(a) indicates the hysteretic behavior of the SMA with inner loops. The time history of the displacement and stress of the midpoint are illustrated in Figures 9(b) and 9(c),

respectively. Finally, Figure 9(d) shows the amount of the dissipated energy in the SMA beam versus time for the forced vibration. From Figures 9(b) and (d), it could be realized that the area of the dissipated energy reduces and consequently, the reduction rate of the vibration amplitude decreases too. With continuing vibration, the beam will oscillate with a constant amplitude. In other words, according to the hysteresis phenomenon of the SMA, the amplitude initially tends to decrease as well as approach to the elastic situations and after that, indicate a constant response.

3. 3. Parametric Analysis Here, the vibrational behavior of the SMA beam is analyzed to evaluate the influence of system parameters such as the spring constant, excitation force magnitude and excitation force frequency on the displacement and stress of the midpoint.

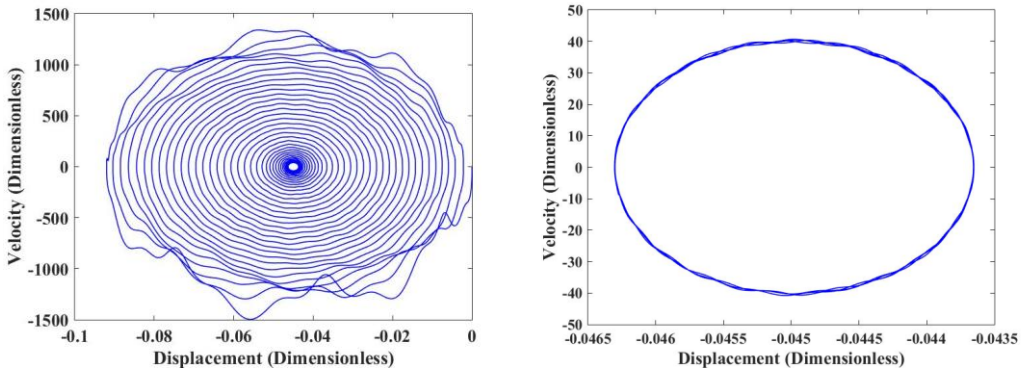

Figure 8. Phase plane diagrams corresponding to free vibration of the midpoint of the beam for $f_0 = -15(N)$: (a) $\tau = 1:400$, (b) $\tau = 380:400$

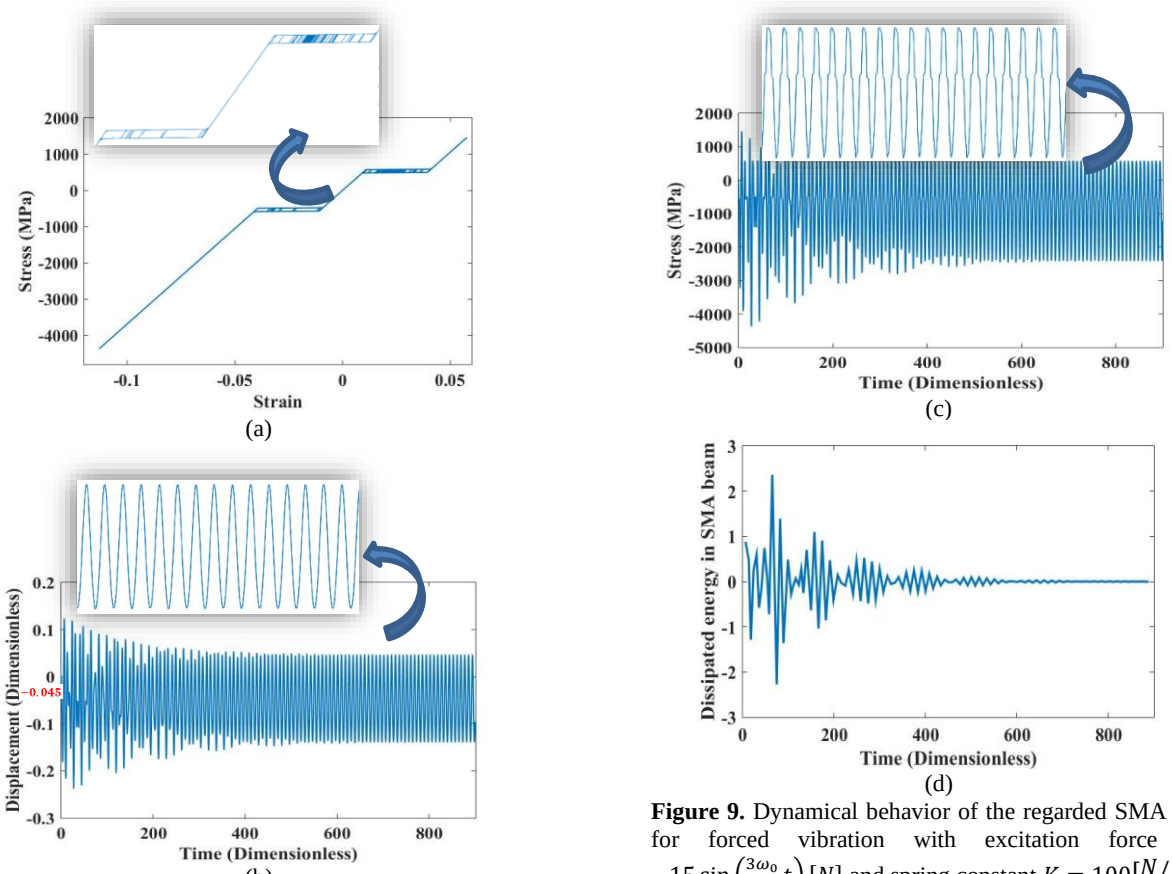

Figure 9. Dynamical behavior of the regarded SMA beam for forced vibration with excitation force $F = -15\sin\left(\frac{3\omega_0}{4}t\right)[N]$ and spring constant $K = 100[N/mm]$

In this way, the results in Figure 11 show that by increasing the value of spring constant K, the vibration amplitude and the stress at the midpoint are reduced, while the frequency of the vibration is increased. Therefore, it can be realized that the spring constant has a great effect on the vibration response of the beam. Moreover, Figure 12 exhibits the results of the forced vibration at the midpoint of the SMA beam with different values of the excitation force frequency. Figures 13 and 14 depict the variations of the oscillation amplitude when the excitation force has different values of magnitude and frequency, respectively. As it is understood from Figure 13, by increasing the magnitude of the excitation force, the oscillation amplitude would be increased, too. Besides, it can be observed from Figure 14 when the frequency of the excitation force coincides with the natural frequency ($\omega = \omega_0 = 0.1587$), the oscillation amplitude reaches its maximum value.

Figure 15 presents the energy dissipation rate of the SMA beam for frequency range [0-0.5]. As it is seen from this figure, although the energy dissipation is effective at all frequencies, it is more significant at low frequencies. Indeed, the SMA is potentially a sluggish element and very effective at low frequencies, therefore, it would display a great impact on the energy dissipation at these circumstances. However, it is ideal to have such dominant frequencies, as it can be easily tuned for any system. This frequency could coincide with the natural frequency of the system and prevent from the resonance phenomenon.

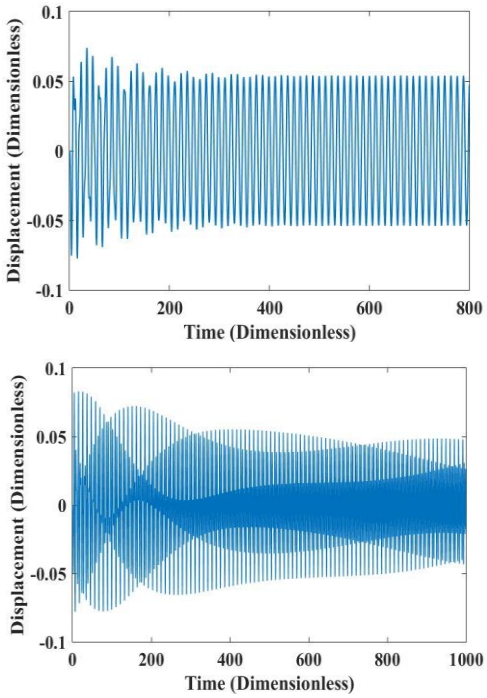

Figure 12. Time responses of the midpoint for different values of the excitation force frequency

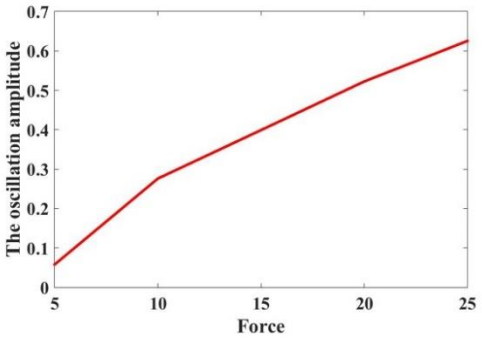

Figure 13. Variations of the oscillation amplitude versus different values of the excitation force magnitude

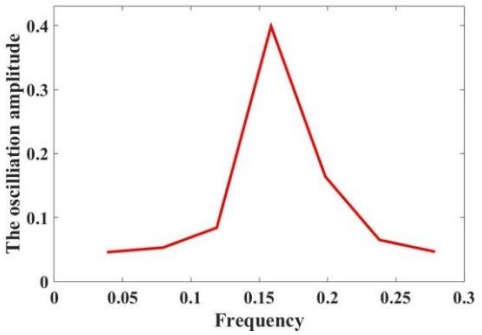

Figure 14. Variations of the oscillation amplitude versus different values of the excitation force frequency

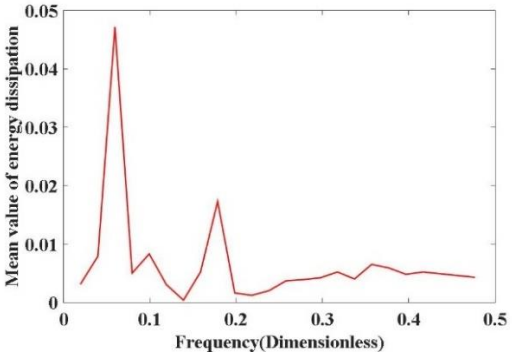

Figure 15. Broad band damping of the SMA beam with the loading condition

In the following, the Discrete Fourier Transformation (DFT) is applied to transform the time domain signal to its representation in the frequency domain. To determine the vibration frequency through the simulation results, the Fast Fourier Transformation (FFT) is implemented to provide the fast computation of the DFT [69]. In this regard, Figure 16 shows the last fourth of the period, regarding the DFT versus the frequency, for the forced vibration in $\omega = \frac{3\omega_0}{4}$Hz. As it can be observed from this diagram, only one frequency component could be

identified, which is about $\omega = 0.119$ Hz. Since this is the oscillation frequency of the SMA beam under the forced vibration, the shape memory alloy has no effect on the frequency of the system.

In Table 2, a comparison is made between the frequencies produced by the FFT and those of the excitation force. As it is observed from these results, the two types of frequencies match well, and the shape memory alloy of the beam has no effect on the frequency of the system.

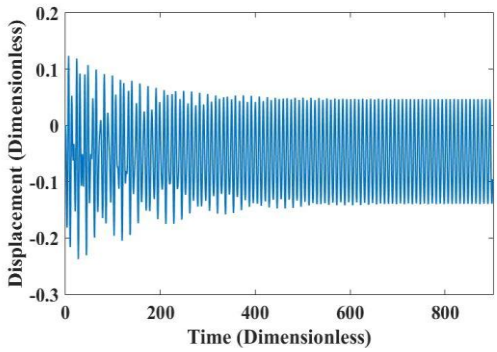

(a)

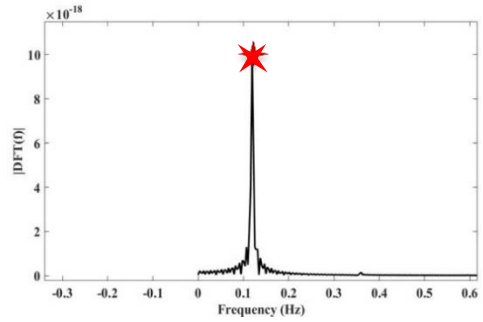

(b)

Figure 16. Simulation results of the SMA beam for forced vibration with $\omega = \frac{3\omega_0}{4}$: (a) time history of the midpoint displacement. (b) Last fourth of the period for the discrete Fourier transformation versus frequency

TABLE 2. Comparisons of the frequencies produced by the FFT and those of the excitation force.

Excitation force frequency	Frequency from FFT	Oscillation amplitude
$\omega = {}^{\omega_0}/_{4}$	0.039	0.046
$\omega = {}^{\omega_0}/_{2}$	0.079	0.053
$\omega = {}^{3\omega_0}/_{4}$	0.119	0.084
$\omega = \omega_0$	0.158	0.399
$\omega = {}^{5\omega_0}/_{4}$	0.198	0.164
$\omega = {}^{3\omega_0}/_{2}$	0.238	0.065
$\omega = {}^{7\omega_0}/_{4}$	0.277	0.047

4. CONCLUSIONS

In this article, the free and forced vibrations of a bending shape memory alloy beam having nonlinear hysteresis, were analyzed regarding the effect of the pseudo-elastic behavior. The three-dimensional constitutive equation of Souza's model was used to simulate the hysteric behavior of the SMA beam.

The time responses and states of strain, transformation strain and stress-strain for the SMA beam were investigated. To shed light on the influences of the SMA on the vibrations, the time histories of the displacement and the stress at midpoint of the beam as well as velocity-displacement and stress- strain diagrams were studied. Moreover, the average of the total dissipated energy was studied for the FFT frequency during the time. The effects of parameters such as the spring constant, excitation force magnitude and excitation force frequency on the displacement and stress of the midpoint were discussed in details. Pursuant to the numerical results, some conclusions could be mentioned as follows.

- The SMA beam exhibits highly nonlinear dynamical behavior.
- The pseudo-elastic behavior of the SMA is a hysteretic energy-dissipation behavior, which causes drastic decreasing in the vibration amplitude of the beam.
- The FFT and excitation force frequencies reveal that the pseudo-elastic behavior of the SMA does not have any effect on the frequency of the system.
- The broad response of the SMA beam due to varying the hysteretic damping with the loading condition displays that it has a great effect on the energy dissipation at low frequencies and could be employed as an effective absorber for slow motion applications.
- The energy absorbing behavior of the SMA beam makes it suitable for suspension systems, or vibrating structures.

5. REFERENCES

1. Kabla, M., Ben-David, E. and Shilo, D., "A novel shape memory alloy microactuator for large in-plane strokes and forces", ***Smart Materials and Structures***, Vol. 25, No. 7, (2016). doi: 10.1088/0964-1726/25/7/075020.
2. Barzegari, M.M., Dardel, M., Fathi, A. and Ghadimi, M., "Aeroelastic characteristics of cantilever wing with embedded shape memory alloys", ***Acta Astronautica***, Vol. 79, (2012), 189-202. doi: 10.1016/j.actaastro.2012.04.023.
3. Pittaccio, S., Garavaglia, L., Ceriotti, C. and Passaretti, F., "Applications of shape memory alloys for neurology and neuromuscular rehabilitation", ***Journal of Functional Biomaterials***, Vol. 6, No. 2, (2015), 328-344. doi: 10.3390/jfb6020328.
4. Sohn, J., Han, Y., Choi, S., Lee, Y. and Han, M., "Vibration and position tracking control of a flexible beam using sma wire

actuators", ***Journal of Vibration and Control***, Vol. 15, No. 2, (2009), 263-281. doi: 10.1177/1077546308094251.

5. She, Y., Chen, J., Shi, H. and Su, H.-J., "Modeling and validation of a novel bending actuator for soft robotics applications", ***Soft Robotics***, Vol. 3, No. 2, (2016), 71-81. doi: 10.1089/soro.2015.0022.
6. Bellini, A., Colli, M. and Dragoni, E., "Mechatronic design of a shape memory alloy actuator for automotive tumble flaps: A case study", ***IEEE Transactions on Industrial Electronics***, Vol. 56, No. 7, (2009), 2644-2656. doi: 10.1109/TIE.2009.2019773.
7. Burugupally, S.P., Koppolu, B., Danesh, N., Lee, Y., Indeewari, V. and Li, B., "Enhancing the performance of dielectric elastomer actuators through the approach of distributed electrode array with fractal interconnects architecture", ***Journal of Micromechanics and Microengineering***, Vol. 31, No. 6, (2021), 064002. doi: 10.1088/1361-6439/abf632.
8. Kang, Z. and James, K.A., "Multiphysics design of programmable shape-memory alloy-based smart structures via topology optimization", ***Structural and Multidisciplinary Optimization***, Vol. 65, No. 1, (2022), 24. doi: 10.1007/s00158-021-03101-z.
9. Ozturk, B., Cetin, H., Dutkiewicz, M., Aydin, E. and Noroozinejad Farsangi, E., "On the efficacy of a novel optimized tuned mass damper for minimizing dynamic responses of cantilever beams", ***Applied Sciences***, Vol. 12, No. 15, (2022), 7878. doi: 10.3390/app12157878.
10. Aydin, E., Öztürk, B. and Dutkiewicz, M., "Analysis of efficiency of passive dampers in multistorey buildings", ***Journal of Sound and Vibration***, Vol. 439, (2019), 17-28. doi: 10.1016/j.jsv.2018.09.031.
11. Aydin, E., Dutkiewicz, M., Öztürk, B. and Sonmez, M., "Optimization of elastic spring supports for cantilever beams", ***Structural and Multidisciplinary Optimization***, Vol. 62, (2020), 55-81. doi: 10.1007/s00158-019-02469-3.
12. Coşkun, S.B., Atay, M.T. and Öztürk, B., "Transverse vibration analysis of euler-bernoulli beams using analytical approximate techniques", ***Advances in Vibration Analysis Research***, Vol. 1, (2011), 22. doi: 10.5772/15891.
13. Rogers, C.A., "Active vibration and structural acoustic control of shape memory alloy hybrid composites: Experimental results", ***The Journal of the Acoustical Society of America***, Vol. 88, No. 6, (1990), 2803-2811. doi: 10919/52280.
14. Peyroux, R., Chrysochoos, A., Licht, C. and Löbel, M., "Thermomechanical couplings and pseudoelasticity of shape memory alloys", ***International Journal of Engineering Science***, Vol. 36, No. 4, (1998), 489-509. doi: doi:10.1016/S0020-7225(97)00052-9.
15. Grabe, C. and Bruhns, O.T., "On the viscous and strain rate dependent behavior of polycrystalline niti", ***International Journal of Solids and Structures***, Vol. 45, No. 7-8, (2008), 1876-1895. doi: 10.1016/j.ijsolstr.2007.10.029.
16. Müller, C. and Bruhns, O., "A thermodynamic finite-strain model for pseudoelastic shape memory alloys", ***International Journal of Plasticity***, Vol. 22, No. 9, (2006), 1658-1682. doi: 10.1016/j.ijplas.2006.02.010.
17. Christ, D. and Reese, S., "A finite element model for shape memory alloys considering thermomechanical couplings at large strains", ***International Journal of Solids and Structures***, Vol. 46, No. 20, (2009), 3694-3709. doi: 10.1016/j.ijsolstr.2009.06.017.
18. Andani, M.T. and Elahinia, M., "A rate dependent tension–torsion constitutive model for superelastic nitinol under non-proportional loading; a departure from von mises equivalency", ***Smart Materials and Structures***, Vol. 23, No. 1, (2013), 015012. doi: 10.1088/0964-1726/23/1/015012.
19. Chatziathanasiou, D., Chemisky, Y., Chatzigeorgiou, G. and Meraghni, F., "Modeling of coupled phase transformation and reorientation in shape memory alloys under non-proportional thermomechanical loading", ***International Journal of Plasticity***, Vol. 82, (2016), 192-224. doi: 10.1016/j.ijplas.2016.03.005.
20. Jani, J.M., Leary, M., Subic, A. and Gibson, M.A., "A review of shape memory alloy research, applications and opportunities", ***Materials & Design (1980-2015)***, Vol. 56, (2014), 1078-1113. doi: 10.1016/j.matdes.2013.11.084.
21. Chemisky, Y., Chatzigeorgiou, G., Kumar, P. and Lagoudas, D.C., "A constitutive model for cyclic actuation of high-temperature shape memory alloys", ***Mechanics of materials***, Vol. 68, (2014), 120-136. doi: 10.1016/j.mechmat.2013.07.020.
22. Plietsch, R., Bourauel, C., Drescher, D. and Nellen, B., "Analytical description of the bending behaviour of niti shape-memory alloys", ***Journal of Materials Science***, Vol. 29, No. 22, (1994), 5892-5902. doi: 10.1007/BF00366873.
23. Auricchio, F. and Sacco, E., "A one-dimensional model for superelastic shape-memory alloys with different elastic properties between austenite and martensite", ***International Journal of Non-Linear Mechanics***, Vol. 32, No. 6, (1997), 1101-1114. doi: 10.1016/S0020-7462(96)00130-8.
24. Rajagopal, K.R. and Srinivasa, A.R., "On the bending of shape memory wires", ***Mechanics of Advanced Materials and Structures***, Vol. 12, No. 5, (2005), 319-330. doi: 10.1080/15376490590953581.
25. Eshghinejad, A. and Elahinia, M., "Exact solution for bending of shape memory alloy superelastic beams", in ASME conference proceedings. Vol. 54723, (2011), 345-352.
26. Rizzoni, R., Merlin, M. and Casari, D., "Shape recovery behaviour of niti strips in bending: Experiments and modelling", ***Continuum Mechanics and Thermodynamics***, (2013), 1-21. doi: 10.1007/s00161-012-0242-0.
27. Mirzaeifar, R., DesRoches, R., Yavari, A. and Gall, K., "On superelastic bending of shape memory alloy beams", ***International Journal of Solids and Structures***, Vol. 50, No. 10, (2013), 1664-1680. doi: 10.1016/j.ijsolstr.2013.01.035.
28. Ostadrahimi, A., Arghavani, J. and Poorasadion, S., "An analytical study on the bending of prismatic sma beams", ***Smart Materials and Structures***, Vol. 24, No. 12, (2015), 125035. doi: 10.1088/0964-1726/24/12/125035.
29. Atanacković, T. and Achenbach, M., "Moment-curvature relations for a pseudoelastic beam", ***Continuum Mechanics and Thermodynamics***, Vol. 1, No. 1, (1989), 73-80. doi: 10.1007/BF01125887.
30. Liu, M.X., J. Li, Q. , "Design and experiment of piezoelectric-shape memory alloy composite shock absorber", ***Materials Letters***, Vol. 304, (2021). doi: 10.1016/j.matlet.2021.130538.
31. Sattari, M.K., M. Akbarzadeh, S. Gholami, R. Beheshti, A. , "Wear in superelastic shape memory alloys: A thermomechanical analysis", ***Wear*** (2022), 488-489. doi: 10.1016/j.wear.2021.204139.
32. De la Flor, S., Urbina, C. and Ferrando, F., "Asymmetrical bending model for niti shape memory wires: Numerical simulations and experimental analysis", ***Strain***, Vol. 47, No. 3, (2011), 255-267. doi: 10.1111/j.1475-1305.2009.00679.x.
33. Hartl, D., Lagoudas, D., Calkins, F. and Mabe, J., "Use of a ni60ti shape memory alloy for active jet engine chevron application: I. Thermomechanical characterization", ***Smart Materials and Structures***, Vol. 19, No. 1, (2009), 015020. doi: 10.1088/0964-1726/19/1/015021.
34. Hartl, D., Mooney, J., Lagoudas, D., Calkins, F. and Mabe, J., "Use of a ni60ti shape memory alloy for active jet engine chevron application: Ii. Experimentally validated numerical analysis", ***Smart Materials and Structures***, Vol. 19, No. 1, (2009), 015021. doi: 10.1088/0964-1726/19/1/015021.

35. Razavilar, R., Fathi, A., Dardel, M. and Arghavani Hadi, J., "Dynamic analysis of a shape memory alloy beam with pseudoelastic behavior", ***Journal of Intelligent Material Systems and Structures***, Vol. 29, No. 9, (2018), 1835-1849. doi: 10.1177/1045389X17754268.
36. Hashemi, S. and Khadem, S., "Modeling and analysis of the vibration behavior of a shape memory alloy beam", ***International Journal of Mechanical Sciences***, Vol. 48, No. 1, (2006), 44-52. doi: 10.1016/j.ijmecsci.2005.09.011.
37. Jose, S., Chakraborty, G. and Bhattacharyya, R., "Coupled thermo-mechanical analysis of a vibration isolator made of shape memory alloy", ***International Journal of Solids and Structures***, Vol. 115, (2017), 87-103. doi: 10.1016/j.ijsolstr.2017.03.001.
38. Pan, Q. and Cho, C., "The investigation of a shape memory alloy micro-damper for mems applications", ***Sensors***, Vol. 7, No. 9, (2007), 1887-1900. doi: 10.3390/s7091887.
39. Damanpack, A., Bodaghi, M., Aghdam, M. and Shakeri, M., "On the vibration control capability of shape memory alloy composite beams", ***Composite Structures***, Vol. 110, No., (2014), 325-334. doi: 10.1016/j.compstruct.2013.12.002.
40. Panico, M. and Brinson, L., "A three-dimensional phenomenological model for martensite reorientation in shape memory alloys", ***Journal of the Mechanics and Physics of Solids***, Vol. 55, No. 11, (2007), 2491-2511. doi: 10.1016/j.jmps.2007.03.010.
41. Brinson, L., Huang, M., Boller, C. and Brand, W., "Analysis of controlled beam deflections using sma wires", ***Journal of Intelligent Material Systems and Structures***, Vol. 8, No. 1, (1997), 12-25. doi: 10.1177/1045389X9700800103.
42. Moallem, M., "Deflection control of a flexible beam using shape memory alloy actuators", ***Smart Materials and Structures***, Vol. 12, No. 6, (2003), 1023. doi: 10.1088/0964-1726/12/6/022.
43. Sayyaadi, H. and Zakerzadeh, M., "Nonlinear analysis of a flexible beam actuated by a couple of active sma wire actuators", ***International Journal of Engineering, Transactions A: Basics***, Vol. 25, No. 3, (2012), 249-264. doi: 10.5829/idosi.ije.2012.25.03a.07.
44. Andrade, B.H., Silva, D.D., Brito, I.C., Caluête, R.E., Sousa, A.R., Gomes, R.M. and Oliveira, D.F., "Influence of strain rate on mechanical properties of a cualmntib shape memory alloy", ***Journal of Materials Research and Technology***, Vol. 16, No., (2022), 1667-1672. doi: 10.1016/j.jmrt.2021.12.100.
45. Billah, A.M., Rahman, J. and Zhang, Q., "Shape memory alloys (smas) for resilient bridges: A state-of-the-art review", in Structures, Elsevier. Vol. 37, (2022), 514-527.
46. Bellini, C., Berto, F., Di Cocco, V. and Iacoviello, F., "A cyclic integrated microstructural-mechanical model for a shape memory alloy", ***International Journal of Fatigue***, Vol. 153, (2021), 106473. doi: 10.1016/j.ijfatigue.2021.106473.
47. Souza, A.C., Mamiya, E.N. and Zouain, N., "Three-dimensional model for solids undergoing stress-induced phase transformations", ***European Journal of Mechanics-A/Solids***, Vol. 17, No. 5, (1998), 789-806. doi: 10.1016/S0997-7538(98)80005-3.
48. Paik, J.K., Hawkes, E. and Wood, R.J., "A novel low-profile shape memory alloy torsional actuator", ***Smart Materials and Structures***, Vol. 19, No. 12, (2010), 125014. doi: 10.1088/0964-1726/19/12/125014.
49. Chung, J.-H., Heo, J.-S. and Lee, J.-J., "Modeling and numerical simulation of the pseudoelastic behavior of shape memory alloy circular rods under tension–torsion combined loading", ***Smart Materials and Structures***, Vol. 15, No. 6, (2006), 1651. doi: 10.1088/0964-1726/15/6/018.
50. Viet, N. and Zaki, W., "Analytical investigation of the behavior of concrete beams reinforced with multiple circular superelastic shape memory alloy bars", ***Composite Structures***, Vol. 210, (2019), 958-970. doi: 10.1016/j.compstruct.2018.11.080.
51. Viet, N. and Zaki, W., "Bending model for functionally graded porous shape memory alloy/poroelastic composite cantilever beams", ***Applied Mathematical Modelling***, Vol. 97, (2021), 398-417. doi: 10.1016/j.apm.2021.03.058.
52. Auricchio, F., Taylor, R.L. and Lubliner, J., "Shape-memory alloys: Macromodelling and numerical simulations of the superelastic behavior", ***Computer methods in applied mechanics and engineering***, Vol. 146, No. 3-4, (1997), 281-312. doi: 10.1016/S0045-7825(96)01232-7.
53. Sun, Q.P. and Hwang, K.C., "Micromechanics modelling for the constitutive behavior of polycrystalline shape memory alloys—i. Derivation of general relations", ***Journal of the Mechanics and Physics of Solids***, Vol. 41, No. 1, (1993), 1-17. doi: 10.1016/0022-5096(93)90060-S.
54. Auricchio, F., Bonetti, E., Scalet, G. and Ubertini, F., "Theoretical and numerical modeling of shape memory alloys accounting for multiple phase transformations and martensite reorientation", ***International Journal of Plasticity***, Vol. 59, (2014), 30-54. doi: 10.1016/j.ijplas.2014.03.008.
55. Arghavani, J., Auricchio, F. and Naghdabadi, R., "A finite strain kinematic hardening constitutive model based on hencky strain: General framework, solution algorithm and application to shape memory alloys", ***International Journal of Plasticity***, Vol. 27, No. 6, (2011), 940-961. doi: 10.1016/j.ijplas.2010.10.006.
56. Gao, X., Huang, M. and Brinson, L.C., "A multivariant micromechanical model for smas part 1. Crystallographic issues for single crystal model", ***International Journal of Plasticity***, Vol. 16, No. 10, (2000), 1345-1369. doi: 10.1016/S0749-6419(00)00013-9.
57. Patoor, E., Lagoudas, D.C., Entchev, P.B., Brinson, L.C. and Gao, X., "Shape memory alloys, part i: General properties and modeling of single crystals", ***Mechanics of Materials***, Vol. 38, No. 5, (2006), 391-429. doi: 10.1016/j.mechmat.2005.05.027.
58. Lagoudas, D.C., Entchev, P.B., Popov, P., Patoor, E., Brinson, L.C. and Gao, X., "Shape memory alloys, part ii: Modeling of polycrystals", ***Mechanics of Materials***, Vol. 38, No. 5, (2006), 430-462. doi: 10.1016/j.mechmat.2005.08.003.
59. Boyd, J.G. and Lagoudas, D.C., "Thermomechanical response of shape memory composites", ***Journal of Intelligent Material Systems and Structures***, Vol. 5, No. 3, (1994), 333-346. doi: 10.1177/1045389X9400500306.
60. Tanaka, K. and Nagaki, S., "A thermomechanical description of materials with internal variables in the process of phase transitions", ***Archive of Applied Mechanics***, Vol. 51, No. 5, (1982), 287-299. doi: 10.1007/BF00536655.
61. Liang, C. and Rogers, C.A., "One-dimensional thermomechanical constitutive relations for shape memory materials", ***Journal of Intelligent Material Systems and Structures***, Vol. 8, No. 4, (1997), 285-302. doi: 10.1177/1045389X9000100205.
62. Brinson, L.C., "One-dimensional constitutive behavior of shape memory alloys: Thermomechanical derivation with non-constant material functions and redefined martensite internal variable", ***Journal of Intelligent Material Systems and Structures***, Vol. 4, No. 2, (1993), 229-242. doi: 10.1177/1045389X9300400213.
63. Ivshin, Y. and Pence, T.J., "A thermomechanical model for a one variant shape memory material", ***Journal of Intelligent Material Systems and Structures***, Vol. 5, No. 4, (1994), 455-473. doi: 10.1177/1045389X9400500402.
64. Ivshin, Y. and Pence, T.J., "A constitutive model for hysteretic phase transition behavior", ***International Journal of Engineering Science***, Vol. 32, No. 4, (1994), 681-704. doi: 10.1016/0020-7225(94)90027-2.
65. Simo, J. and Taylor, R., "A return mapping algorithm for plane stress elastoplasticity", ***International Journal for Numerical***

Methods in Engineering, Vol. 22, No. 3, (1986), 649-670. doi: 10.1002/nme.1620220310.

66. Bertram, A., "Thermo-mechanical constitutive equations for the description of shape memory effects in alloys", ***Nuclear Engineering and Design***, Vol. 74, No. 2, (1983), 173-182. doi: 10.1016/0029-5493(83)90054-7.
67. Leclercq, S., Bourbon, G. and Lexcellent, C., "Plasticity like model of martensite phase transition in shape memory alloys", ***Le Journal de Physique IV***, Vol. 5, No. C2, (1995), C2-513-C512-518. doi: 10.1051/jp4:1995279.
68. Courant, R. and Hilbert, D., "Methods of mathematical physics: Partial differential equations, John Wiley & Sons, (2008).
69. Brigham, E.O. and Morrow, R., "The fast fourier transform", ***IEEE Spectrum***, Vol. 4, No. 12, (1967), 63-70. doi: 10.1109/MSPEC.1967.5217220.

Persian Abstract

چکیده

هدف از این تحقیق معرفی یک رویکرد نیمه تحلیلی برای تحلیل ارتعاشات غیرخطی آزاد و اجباری تیر آلیاژ حافظه دار خمشی (SMA) با در نظر گرفتن تأثیر رفتار شبه الاستیک آن است. به منظور ایجاد یک انحراف اولیه، یک پیش کرنش مناسب با استفاده از فنر فشاری به تیر SMA اعمال می شود. یک مدل ماده جدید برای شبیه‌سازی رفتار هیستریک غیرخطی تیر SMA استفاده می‌شود، در حالی که معادلات دیفرانسیل حرکت تیر بر اساس نظریه تیر اویلر–برنولی و اصل همیلتون نوشته شده‌اند. معادلات دیفرانسیل جزئی غیرخطی استخراج شده با استفاده از روش گالرکین و به صورت نیمه تحلیلی حل می‌شوند. رفتار شبه الاستیک و اتلاف انرژی تیر SMA در وضعیت‌های ارتعاش غیرخطی آزاد و اجباری مورد مطالعه قرار می‌گیرد. در نهایت، تأثیر پارامترهای سیستم مانند ثابت فنر، دامنه و فرکانس نیروی تحریک بر راندمان جاذب بررسی شده و پایداری آن مورد بررسی قرار می‌گیرد. نتایج عددی نشان می‌دهد که تیر SMA رفتار دینامیکی بسیار غیرخطی از خود نشان می‌دهد و می‌تواند به عنوان یک محرک برای میرایی انرژی استفاده شود.